

# We are IntechOpen, the world's leading publisher of Open Access books Built by scientists, for scientists

6,900

Open access books available

186,000

International authors and editors

200M

Downloads

Our authors are among the

154

Countries delivered to

TOP 1%

most cited scientists

12.2%

Contributors from top 500 universities



WEB OF SCIENCE™

Selection of our books indexed in the Book Citation Index  
in Web of Science™ Core Collection (BKCI)

Interested in publishing with us?  
Contact [book.department@intechopen.com](mailto:book.department@intechopen.com)

Numbers displayed above are based on latest data collected.  
For more information visit [www.intechopen.com](http://www.intechopen.com)



# The Use of a Spiral Band Model to Estimate Tropical Cyclone Intensity

*Boris Yurchak*

## Abstract

Spiral cloud-rain bands (SCRBs) are some of the most distinguishing features inherent in satellite and radar images of tropical cyclones (TC). The subject of the proposed research is the finding of a physically substantiated method for estimation of the TC's intensity using SCRBS' configuration parameters. To connect a rainband pattern to a physical process that conditions the spiraling feature of a rainband, it is assumed that the rainband's configuration near the core of a TC is governed primarily by a streamline. In turn, based on the distribution of primary forces in a TC, an analytical expression as a combination of hyperbolic and logarithmic spirals (HLS) for the description of TC spiral streamline (rainband) is retrieved. Parameters of the HLS are determined by the physical parameters of a TC, particularly, by the maximal wind speed (MWS). To apply this theoretical finding to practical estimation of the TC's intensity, several approximation techniques are developed to "convert" rainband configuration to the estimation of the MWS. The developed techniques have been tested by exploring satellite infrared imageries and airborne and coastal radar data, and the outcomes were compared with in situ measurements of wind speeds and the best track data of tropical cyclones.

**Keywords:** hyperbolic-logarithmic spiral, tropical cyclone, spiral cloud-rain bands, maximum wind speed, approximation

## 1. Introduction

The issue addressed in this chapter relates to methods for estimating the intensity of a tropical cyclone (TC) from the characteristics of its cloud-rain field (CRF) structure. In general, these methods are empirical and semiempirical, i.e., they are based on the correlation of the structural features of the CRF with the intensity of the TC found from observations from satellites and radars. The most widely used method in operational practice is the Dvorak method [1, 2]. This chapter relates to the exploring of one of the most pronounced structural elements of the CRF, which are spiral cloud-rain bands (SCRBs). Attention was first attracted to these bands by Wexler [3] based on aircraft observations. It was suggested that SCRBS indicate the mature cyclone and its organization follows the streamlines. The authors of [4] described the SCRBS observed on the radar and suggested to use a modified logarithmic spiral to express its configuration in mathematic form. Although SCRBS have been studied for a long time, there is currently no consensus about their origin

and mechanism of generation. Reviews of proposed hypotheses are given in [5–8]. In the paper of Lahiri [9], a first attempt was undertaken to estimate the effect of the TC intensity on the geometric characteristics of SCRBs. In this study, a simple model of a TC in which the low-level streamlines were described by logarithmic spirals was suggested. It was shown that the rate of generation of a latent heat in the model was proportional to the crossing angle that is a parameter of the spiral. (As follows from [4], the “crossing angle” of a SCRB of a finite width is the angle at which the longitudinal axial curve of the SCRB crosses the concentric circle (centered at the center of the cyclone) at a given arbitrary point belonging to the axial curve; that is, this is the angle between the tangents to the axial curve and the said circle at this point). As a result, crossing angle decreases as cyclones matured since the latent heat is very small in this stage. However, no relationship between the maximum wind speed (MWS) and the crossing angle was obtained. Moreover, the description of SCRBs by a logarithmic spiral only is an internally contradictory approximation due to the following circumstances. On the one hand, the main property of the logarithmic spiral is the constancy of the crossing angle for any of its points. Therefore, in particular, the alternative name of this spiral is an equiangular spiral. On the other hand, it was found that the crossing angle is sensitive to wind speed. But wind speed is not constant along the SCRB. Therefore, the crossing angle cannot have a constant value along the SCRB as well. Thus, the main feature of the logarithmic spiral (constancy of the crossing angle) is not consistent with the physics of the process. In the modified logarithmic spiral [4], the experimentally observed dependence of the crossing angle on distance is taken into account by introducing a radius of so-called inner limiting circle, at which the crossing angle is zero. However, the relationship of this radius with the intensity of the cyclone and the radius of the maximum wind (RMW) has not been established. It should be noted that the “spiralness” of the SCRB is also used in the empirical Dvorak method, although only at the qualitative level, by estimating the sector occupied by the spiral structure (“count the tenths” method), which is approximated by a logarithmic spiral with the crossing angle of  $10^\circ$ . However, as it was stated in [10], this spiral does not have a physical basis. In our papers [11–14], the assumption of authors [3, 4, 9] that rainbands are well arranged along streamlines was also used. In general, this assumption is confirmed by a comparison of radar and aircraft data (e.g., [15, 16]). The same orientation of the principal rainband along the jet is demonstrated in [7]. Further, the expression for spiral streamline has been derived in [11] in the closed form as hyperbolic-logarithmic spiral (HLS). The most advantage feature of the HLS is the dependence of one of its parameters on the MWS. Unlike the previous studies, the HLS was not assumed but was accurately derived based on physical considerations. At the same time, it turned out that only the peripheral portion of the HLS is similar to the logarithmic spiral. The size of this portion and the corresponding crossing angle are determined by the parameters of the cyclone, including the MWS. Unlike the modified logarithmic spiral, the change in the tangent of the crossing angle in the HLS is governed not by the distance weight function (equal to zero at the distance equal to the radius of the inner limiting circle and approaches unity at the outer edge of the cyclone), but by the physical parameters of the cyclone. However, it is not possible to determine the MWS by the crossing angle of the logarithmic section of the HLS only, as well, due to multifactor influence on the crossing angle. On the other hand, approximation of a SCRB by the HLS allows determining the MWS based on the known characteristics of the cyclone in cases when the SCRB is sufficiently long and markedly different from the logarithmic spiral. A discussion of the physical basis of the proposed method, methodology, and results of its application is the subject of this chapter. In particular, the derivation of the HLS based on the distribution of forces affecting

the cyclone, methods for approximating the SCRB, the results of estimating the MWS from radar, and satellite data in comparison with the data of direct measurements and final conclusions of the corresponding meteorological services (Best Track reports) are provided.

## 2. Hyperbolic-logarithmic model of a streamline in a cyclone

### 2.1 Streamline equation in polar coordinates

As per Batchelor [17], radial ( $v$ ) and tangential ( $u$ ) components of a fluid flow are respectively:

$$v = \frac{1}{r} \frac{d\psi}{d\varphi}, \tag{1}$$

$$u = -\frac{d\psi}{dr}, \tag{2}$$

where  $r$  and  $\varphi$  are polar radius and polar angle, respectively, and  $\Psi$  is the stream function. The combination of (1) and (2) results the streamline equation in polar coordinates:

$$-r \frac{d\varphi}{u} = \frac{1}{v} dr. \tag{3}$$

Considering  $\frac{u}{v} = \tan(\mu)$ , where  $\mu$  is the inflow angle (**Figure 1**), the final form of the streamline equation is

$$-\frac{d\varphi}{dr} = \frac{1}{r} \tan \mu(r) \tag{4}$$

It should be noted that the sum of inflow and crossing angles is the right angle (**Figure 1**).

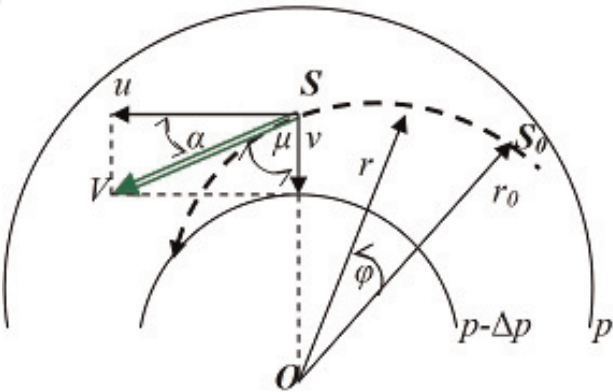


**Figure 1.**  
To the derivation of the streamline equation.  $\alpha$  is the crossing angle;  $\mu$  is the inflow angle; the bold dashed curve is the streamline; solid curves designate  $p$  and  $p-\Delta p$  isobars ( $p$  is the pressure,  $\Delta p$  is the pressure change between isobars);  $V$  is the wind speed of air in point  $S$ ;  $u$  and  $v$  are tangential and radial components of the wind speed  $V$  at point  $S$ , respectively; and  $\varphi$  is the polar angle of radius vector  $r$  counted off from arbitrary selected point  $S_0$ .

## 2.2 Inflow angle from the balance of forces in a cyclone

To express the streamline Eq. (4) through the physical parameters of a cyclone, the inflow angle should be evaluated based on the balance of forces in a cyclone. The diagram of forces is depicted in **Figure 2** as follows from [18].

The balance condition called Guldberg-Mohn balance [19] is expressed as follows:

$$F_G = F_B \quad (5)$$

where

$$F_G = -\frac{1}{\rho} \frac{\partial p}{\partial r} \quad (6)$$

is the gradient force ( $\rho$  is the air density);

$$\vec{F}_B = \vec{F}_c + \vec{F}_d + \vec{F}_R \quad (7)$$

is the balancing force containing

$$F_c = \frac{V^2}{r}, \quad (8)$$

which is the centrifugal force;

$$F_d = V \cdot f, \quad (9)$$

which is the deflecting force ( $f = 2\omega \sin \phi$  is the Coriolis parameter,  $\omega$  is the angular speed of the Earth rotation, and  $\phi$  is the altitude); and

$$F_R = -k \cdot V, \quad (10)$$

which is the frictional force, where  $k$  is the friction factor ( $s^{-1}$ ). All forces in the above expressions (8)–(10) are given per unit mass. As it follows from **Figure 2** and Eqs. (8)–(10), the tangent of inflow angle under the steady-state air movement in the friction layer is defined by a relationship:

$$\tan \mu(r) = \frac{F_c + F_d}{|F_R|} = \frac{f}{k} + \frac{V(r)}{kr}. \quad (11)$$

## 2.3 The streamline equation as a function of physical parameters of a cyclone

Let us assume for definiteness that the speed of wind  $V(r)$  changes with cyclone radius in accordance with a power law which is inherent to the Rankine vortex [20]:

$$V(r) = V_m \left( \frac{r_m}{r} \right)^n, \quad r \geq r_m, \quad (12)$$

where  $V_m$  is the MWS,  $n$  is the exponent (hyperbolic index), and  $r_m$  is the radius of the maximum wind (RMW). Under these conditions, Eq. (4) can be written as

$$-d\phi = \left( \frac{B}{r} + b \frac{1}{r^{n+2}} \right) dr, \quad (13)$$

where

and

5

Using the Maclaurin series expansion for an exponential function  $\left(e^x = \sum_{i=0}^{\infty} x^i / i!\right)$  and combining the coefficients at the argument of the first power, Eq. (19) can be written as a polynomial:

$$\varphi = A \sum_{i=2}^{\infty} \frac{\{-(n+1)\}^i}{i!} (\ln y)^i - \{A(n+1) + B\} \ln y \quad (20)$$

As follows from Eq. (20), the HLS contains linear and nonlinear parts in regard to the logarithm of the relative polar radius ( $\ln y$ ). Taking into account the expression for coefficient  $A$  (18), the linear part is the logarithmic spiral ( $\varphi_L$ ) that can be expressed in the form:

$$\varphi_L = -\{A(n+1) + B\} \ln y = -\left(\frac{r_m^n}{k r_0^{n+1}} V_m + B\right) \ln y = -B \left(y_m^n \frac{V_m}{V_C} + 1\right) \ln y \quad (21)$$

where  $V_C = f r_0$  is the Coriolis speed at distance  $r_0$  and  $y_m = r_m / r_0$  is the relative RMW. As follows from Eq. (21), the tangent of the crossing angle of the linear part of the HLS depends on many factors as follows:

$$\tan \alpha = \left\{ B \left( y_m^n \frac{V_{\max}}{V_C} + 1 \right) \right\}^{-1}. \quad (22)$$

## 2.5 Graphical representations of HLS streamline

To illustrate the dependence of HLS primary features versus the MWS and the friction factor, the graphical diagrams in polar coordinates (**Figure 3**) and semilogarithmic coordinates (**Figure 4**) for three values of MWS and two values of the friction factor are provided below.

**Figure 3** reflects the known feature of a rainband, as it has been summarized by Willoughby [16]. A rainband of a cyclone from the periphery to its center is curved, due to the increase in the angular velocity, and therefore can be transformed into a logarithmic spiral. As the intensity of a cyclone increases, the slope of the twist decreases, and the band configuration becomes like a circular arc. Indeed, the HLS is similar to a logarithmic spiral, but only on the periphery of a cyclone, as shown in Eq. (20), where the normalized polar radius ( $y$ ) is a little less than 1. Toward the center of the cyclone ( $y < 1$ ), the first term in Eq. (20) begins to prevail over the second one, and the HLS begins to “round off” (with constant  $k$  and  $n$ ) accordingly with the observations. The distance where it happens depends on the parameter ratio between the linear and nonlinear parts of Eq. (20). Plots of HLS with  $V_m = 40 \text{ m s}^{-1}$  are missing in **Figure 4** to simplify its reading. In the semilogarithmic coordinates in **Figure 4**, the canonical logarithmic spiral  $\varphi = -(\tan \alpha)^{-1} \cdot \ln y$  would be depicted as a straight line with the angle coefficient equal to the inverse value of the tangent of the corresponding crossing angle. As follows from the plots in **Figure 4**, the HLS is more similar to the logarithmic spiral (straight line) within one turn ( $2\pi$ ), and for  $0.1 \leq y \leq 1$  ( $-2.3 \leq \ln y \leq 0$ ) for any MWS, the greater is the friction factor (compare lower and upper pairs of curves). For small friction factor, the greater the MWS is, the shorter the linear part of the HLS (logarithmic) is (compare two lower curves). As follows from Eq. (22), in contrast to the canonical logarithmic spiral mentioned above where  $\tan \alpha = \text{const}$  at any  $y$ , the tangent of the crossing angle of the HLS linear part depends on the term  $y_m^n V_m / V_C$ . It is a reason

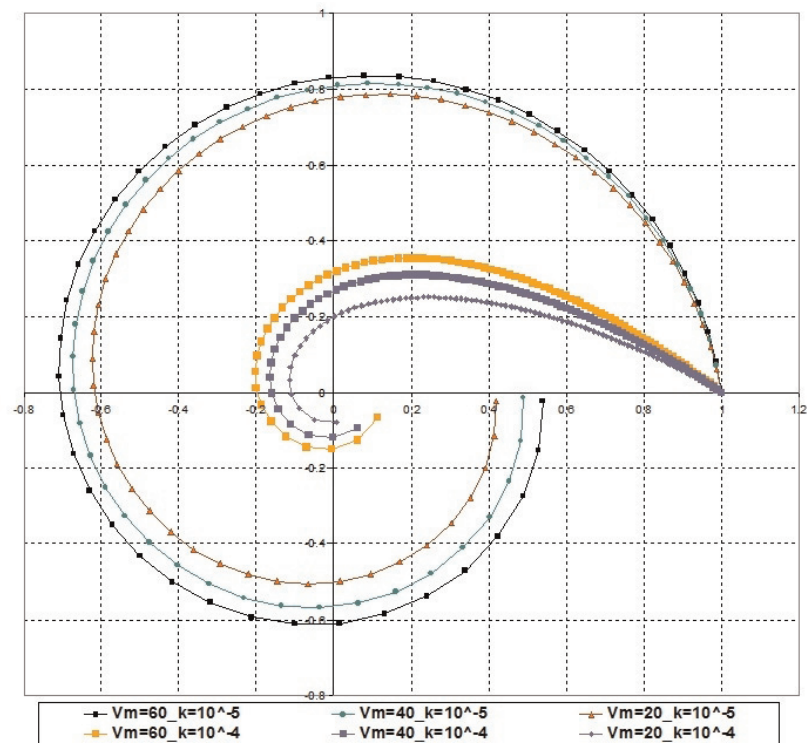


**Figure 3.**  
Illustration of HLS configuration in polar coordinates versus variable maximal wind speed and friction factor; ordinate and abscissa axis are relative polar radius ( $y$ );  $V_m(m\ s^{-1})$ ,  $k\ (s^{-1})$ ,  $r_o = 500\ km$ ,  $n = 0.6$ ,  $y_m = 0.1$ , and  $f = 1 \cdot 10^{-5}\ s^{-1}$  (latitude =  $20^\circ\ N$ ).

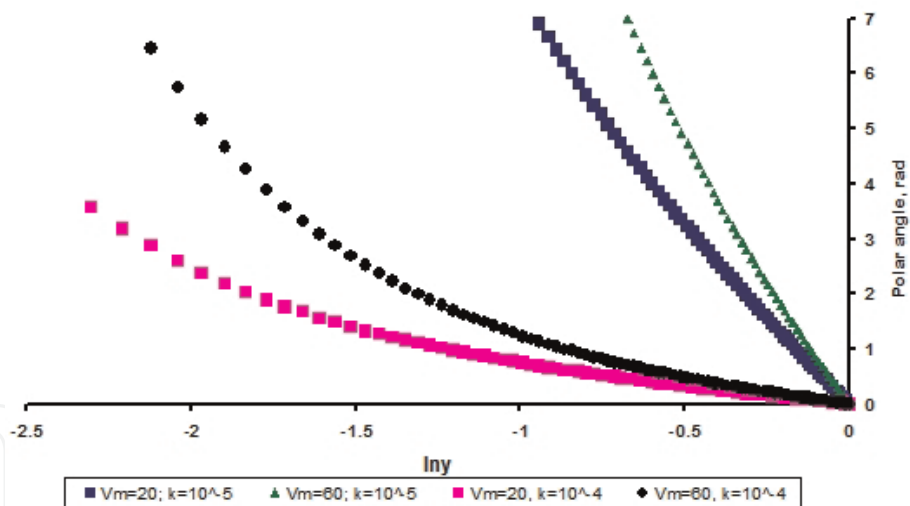


**Figure 4.**  
Illustration of HLS configuration in semilogarithmic coordinates versus variable maximal wind speed and friction factor;  $V_m(m\ s^{-1})$ ,  $k\ (s^{-1})$ ,  $r_o = 500\ km$ ,  $n = 0.6$ ,  $y_m = 0.1$ , and  $f = 1 \cdot 10^{-5}\ s^{-1}$  (latitude =  $20^\circ\ N$ ).

why the linear parts of pairs of curves in **Figure 4** with the same friction factor ( $k = 10^{-5}\ s^{-1}$  or  $k = 10^{-4}\ s^{-1}$ ) and the same Coriolis parameter ( $f$ ) have notable different tilts for different MWS. It is the explanation of the well-known experimental fact, mentioned in the Introduction section, regarding the sensitivity of the crossing angle on the intensity of a TC.

### 3. HLS approximation techniques

The task of using the analytical expression of the streamline (17) or (19) considered in the previous section is to use it to determine the MWS in a TC. The base for

resolving this task is the expression (18) for the coefficient  $A$  that included the MWS. From this expression, taking into account the relationship between the friction coefficient and the coefficient  $B$  (14), one can get the desired formulae for calculation the MWS using the HLS parameters:

$$V_m = A \frac{k(n+1)r_0^{n+1}}{r_m^n} = \frac{A f(n+1)r_0^{n+1}}{B r_m^n} = \frac{A}{B} (n+1) y_m^{-1} V_C \quad (23)$$

Thus, the MWS can be estimated by approximating the SCRB of the TC with the HLS Eq. (19). Under this approximation, values of  $A$  and  $B$  are determined, assuming the value of the hyperbolic index  $n$ , as well as the measured or estimated value of the MWR. Coriolis velocity ( $V_C$ ) is determined by known latitude of the center of the TC and the radius of given initial point of the SCRB. To get the approximation estimate of the HLS coefficients, the standard least squares method (LSM) and the assimilation technique were considered and tested. Brief descriptions of these techniques are provided below.

### 3.1 Estimation of coefficients of the HLS by the least squares method

#### 3.1.1 Relationships for calculation

Taking the exponentially logarithmic form of the HLS (19) and denoting  $\ln y = x$  and  $T(x) = e^{-(n+1)x} - 1$ , it is possible to write

$$\varphi = A \cdot T(x) - B \cdot x. \quad (24)$$

Performing the routine LSM procedure, one gets the calculation relationships for the HLS coefficients estimates which are provided below in the Gauss designation ( $[s] = \sum s$ )

$$\tilde{A} = \frac{1}{D} \{ [x^2] \cdot [\varphi \cdot T(x)] - [x \cdot T(x)] \cdot [\varphi \cdot x] \}, \quad (25)$$

$$\tilde{B} = \frac{1}{D} \{ [x \cdot T(x)] \cdot [\varphi \cdot T(x)] - [T^2(x)] \cdot [\varphi \cdot x] \}. \quad (26)$$

where

$$D = [T^2(x)] [x^2] - [x \cdot T(x)]^2. \quad (27)$$

The error estimates of the coefficients are equal:

$$\sigma_A = \sigma \cdot \sqrt{Q_{11}}, \quad (28)$$

$$\sigma_B = \sigma \cdot \sqrt{Q_{22}}, \quad (29)$$

where

$$\sigma = \sqrt{\frac{[\Delta\varphi^2]}{N-2}}, \quad (30)$$

is the residual variance, where

$$[\Delta\varphi^2] = \sum_{i=1}^N \left( \varphi_{i, \text{exper.}} - \varphi_{i, \text{approx.}} \right)^2 = \sum_{i=1}^N \left( \varphi_{i, \text{exper.}} - \tilde{A} \cdot T(x_i) + \tilde{B} \cdot x_i \right)^2 \quad (31)$$

and terms in (28) and (29) are  $Q_{11} = \frac{[x^2]}{D}$ ,  $Q_{22} = \frac{[T^2(x)]}{D}$ .

### 3.1.2 The condition of stationarity under the application of the LSM for approximation of a SCRB with the HLS

As follows from Eq. (18), coefficient  $A$  of the HLS depends on the selection of radius  $r_0$ . On the other hand, based on the physical sense, the cyclone's physical parameters evaluated from coefficients  $A$  and  $B$  must not depend on selection of the initial point (point of spiral reference). To satisfy this requirement, the selected spiral signature should be fitted by the HLS with coefficient  $A$  that should be proportional to the polar radius with power  $-(n + 1)$  (in accordance with Eq. (18)) and coefficient  $B$  that should be a constant (in accordance with (14)). This validates the fitting of a given spiral signature by the HLS. Substantiation of these conditions, which characterize the "HLS stationarity" and the control technique, is provided below. The term "HLS stationarity" can be explained by providing the following example. Suppose some spiral signature is introduced by a set of point coordinates. This set of points is aimed to be approximated by the HLS using the LSM. Let us select arbitrary the first starting point of approximation (SPA) at the peripheral part of the spiral signature. Suppose its polar radius is  $r_{0,1}$ . The applied LSM procedure evaluates parameters  $A_1$  and  $B_1$ . Next, the another SPA is taken with  $r_{0,2} < r_{0,1}$ . The approximation procedure is repeated, and the second set of parameters  $A_2$  and  $B_2$  is obtained. Taking consequently SPAs along the signature and applying the LSM approximation procedure, the number of sets of  $A_i$  and  $B_i$  can be obtained. It should be noted that the MWS  $V_m$ , the RMW  $r_m$ , friction factor  $k$ , exponent  $n$ , and the Coriolis parameter  $f$  are the same for all approximation runs and different SPAs. Because of that, the values of the HLS coefficients pertained to different sets of evaluated data should satisfy the relationships:

$$A_i y_{0,i}^{n+1} = A_{y,i} = \frac{y_m^n}{k(n+1)r_{0,0}} V_m = A_y, \quad (32)$$

$$B_i = \frac{f}{k} = B, \quad (33)$$

where  $A_y$  and  $B$  are constants pertained to the given spiral element,  $r_{0,0}$  is the polar radius of remotest SPA where the spiral signature can be described by the HLS,  $y_m = r_m/r_{0,0}$ , and  $y_{0,i} = r_{0,i}/r_{0,0}$ . Relationships (32) and (33) together combine the condition of the HLS stationarity. That is, if a spiral signature is really described by the HLS, then the parameters  $A_{y,i}$  and  $B_i$  should be independent (theoretically) on selection of the SPA. Let us assume that the stationarity condition is satisfied within a polar radius range that corresponds to SPAs of indexes from  $i_s$  to  $i_e$ . The definition of the stationary part above is related to the general case, where a spiral signature is represented by  $N$  points with numbers  $i = 1, 2 \dots i_s \dots i_e \dots N$ . The first SPA that is remotest from the center of the cyclone ( $i = 1$ ) is selected arbitrarily, and a SPA with index  $i_s$  has polar radius  $r_{0,0}$ . This ordered nest of point coordinates, where the polar radii of the points are normalized by a distance from the remotest SPA, combines the normalized profile (NP) of a spiral signature. A logarithmic modification of NP, where relative radii are substituted by their natural logarithms, i.e.,  $\varphi_i = f(\ln y_i)$ , is a logarithmic NP (LNP). The sequential

approximation of a spiral signature is performed by the selection of consequent SPAs toward the cyclone center by a given number of points. The deficiencies of conditions (32) and (33) are primarily due to two reasons. The starting of a nonstationary part of a spiral signature  $\{i = 1 \dots (i_s - 1)\}$  is due to the incorrect tracing of streamlines by clouds or the deviation of a streamline from the theoretical HLS for some reason. Regarding the “floor bounding” of the stationary part under SPA with  $i \geq i_e + 1$ , it is possible to show that this feature is due to the change of wind and friction regimes near the area of maximum winds. Beginning from this point, the increase of wind speed becomes slower than that of power  $n_{opt}$ . It might be assumed also that due to high wind speed, the friction factor becomes lower [21] or its dependence on wind speed becomes not linear. At that, the approximation estimates of the HLS coefficients were conducted under  $n_{opt}$  divergent from their stationary values,  $\tilde{B}(n_{opt}) \rightarrow \infty$  and  $\tilde{A}_y(n_{opt}) \rightarrow 0$ . Therefore, the HLS coefficients should be selected from the results of the approximation of a spiral signature within a range where the stationary condition is satisfied. On the other hand, the distance from the center, where such divergence occurs, can be taken as an additional parameter of the cyclonic vortex (radius of divergence). Simulation experiments validated the stationarity and “divergent” property of the HLS coefficients.

### 3.1.3 An example of HLS approximation with LSM

As an example of the application of the above approach to the approximation of the SCRB by the HLS, we consider the estimate of the MWS from an image from the geostationary satellite GMS-5 in the visible range of TC Mitag, at 01:31 UTC on March 5, 2002 (**Figure 5**).

The corresponding logarithmic normalized profile of the annotated signature is shown in **Figure 6**.

As can be seen from **Figure 6**, the “regularity” of the profile is broken in the range  $\ln y = (-0.6) - (-0.7)$ . Apparently this is due to not quite correct annotation of the final segment of the SCRB. It would have to be carried out along the steeper contrast border observed in this area. Therefore, the main part of the profile in the range  $\ln y = 0 - (-0.7)$  was subjected to approximation, only. The main characteristics of the signature were radius of the most distant starting point of the signature  $r_0 = 447$  km,  $r_m = 130$  km, and  $f = 3.3 \cdot 10^{-5} \text{ s}^{-1}$  (latitude  $13.29^\circ\text{N}$ ). As the consecutive

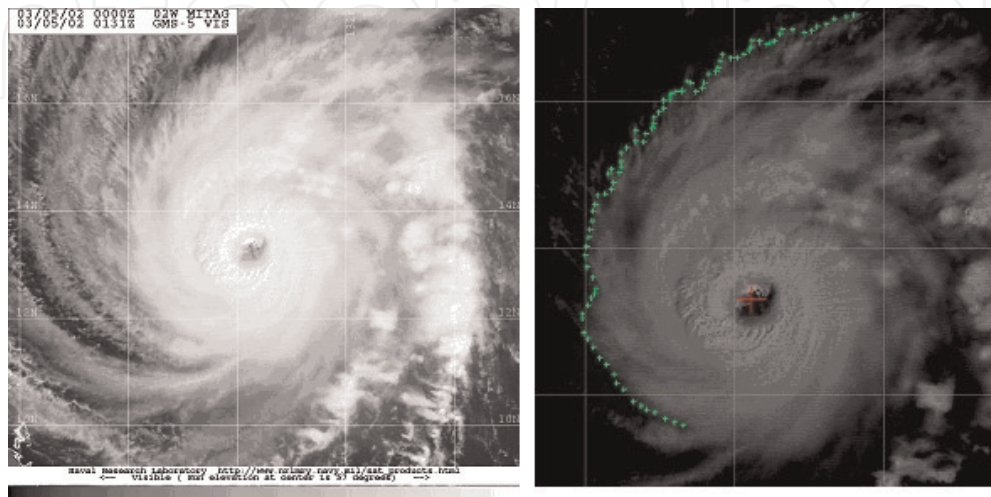


**Figure 5.** Image of TC Mitag (2002) in visible range; left image—original image; right snapshot—a contrasted image with an annotated position of the center of the eye and annotated outer edge of the SCRB adjacent to the cyclone core.

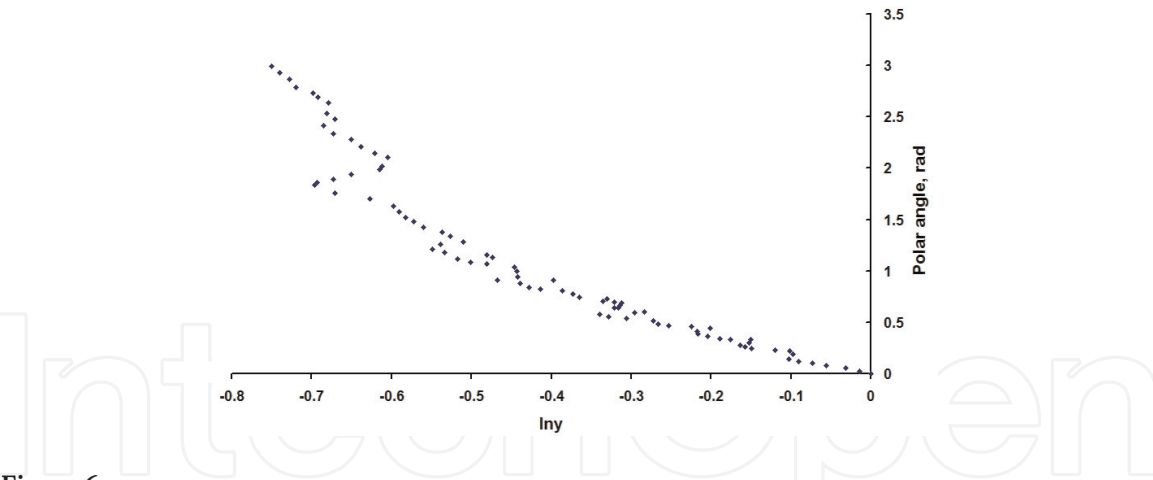


**Figure 6.**  
Logarithmic normalized profile of SCRB annotated in **Figure 5** (right snapshot).

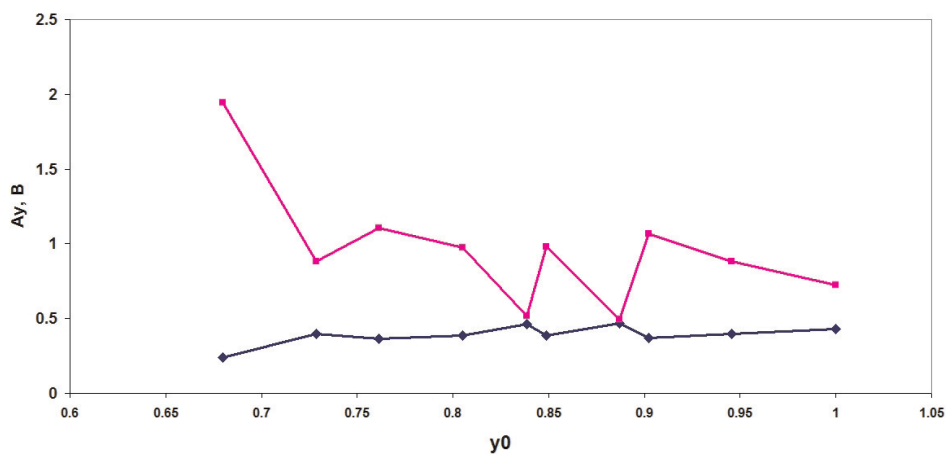


**Figure 7.**  
Graph of stationarity of HLS approximation at  $n = 1.1$ .

tests showed, the stationarity conditions were best performed for both HLS coefficients in this particular case with the hyperbolic index  $n = 1.1$  (**Figure 7**).

The average values of the coefficients  $A_y$  and  $B$  in the stationary segment were  $A_y = 0.41 \pm 0.04$  and  $B = 0.85 \pm 0.22$ , which corresponds to  $V_m = 58.1 \pm 16.1 \text{ ms}^{-1}$ . The meteorological assessment of the TC intensity for this point in time was 115 kts ( $59.2 \text{ ms}^{-1}$ ), which can be considered a satisfactory coincidence even taking into account the difference in altitudes for which the meteorological assessment is made (10 m) and the upper boundary of clouds for which the HLS estimate was calculated. According to experimental data, the MWS in a TC is observed at the level of 850–900 hPa:  $V_m(850 \text{ hPa})$  [22]. The average speed at the level of cloud top  $V_m(240 \text{ hPa})$  makes up about 70–80% of  $V_m(850 \text{ hPa})$  [22, 23]. The surface wind speed (at 10 m height) is smaller than  $V_m(850 \text{ hPa})$  by about 25–30% [24]. Therefore, considering that the configuration of the spiral signature depends on wind speed at the height of its existence, the HLS estimates can be compared (as a first guess) with surface data of meteorological services.

### 3.2 Assimilation technique

#### 3.2.1 Motivation

As follows from the previous section, for the HLS approximation of SCRB by the LSM with the subsequent checking for stationarity, a lot of operations are needed to be performed. This requires considerable time and, therefore, is unlikely to have a

prospect for use in operational practice. In addition, annotation of the spiral structure on the image is, to a certain extent, a subjective process as was shown by the example of **Figure 6**. Moreover, sometimes, as was shown in [11], the LSM approximation leads to nonphysical values of HLS coefficients due to incorrect annotation of the spiral structure. The main problem of the HLS approximation with the LSM is that, by its nature, this technique is applicable mainly to so-called thin or clearly depicted spiral structures, which have a small width or sharp contour in satellite or radar images, and are suitable for its uniquely annotation. However, the same thin spiraling bands very often turn out to be squall lines, which are not related to streamlines. These circumstances stimulated the search for another technique that would be applicable to typical SCRBs, having a noticeable width and fuzzy contours. This technique, called the assimilative technique, is discussed below.

### 3.2.2 A principle of assimilative technique

When choosing a technique for determining the HLS coefficients (3) and (4), it should be noted that a spiral rainband observable on a radar image has a finite width and is a mapping of the resultant involvement of cloud-rain particles in the region affected by the streamline. In this case, parameters of the HLS describing all possible streamlines within the rainband should be considered as “equally possible.” In this technique, an approach based on the allocation of HLSs “fitting” into geometric boundaries of a rainband and determining the “expected” (mean) and “modal” HLSs was used. The fitting spirals were designated as “signatural” HLSs. The signatural HLSs have coefficients  $A$  (3) and  $B$  (4) which are determined using different combinations of  $V_m$ ,  $k$ , and  $n$ . This triplet of parameters is hereafter referred to by the term “physical characteristics.” The mean and modal values of a selected physical parameter over all signatural HLSs are taken as the corresponding statistical estimates of this parameter. The above procedure is called “assimilative HLS approximation.” For the first time, this technique was used for processing of satellite infrared images of a TC in [13]. Further, it was improved in [14]. The primary changes in enhanced technique are the limitation of a range of possible maximum wind speeds resulted from the spiral band processing and finding the modal value of  $V_m$  distribution over all signatural HLSs in addition to the mean value. The technique was called “assimilative” due to a priori assignment of the type of the approximating function (HLS) and the range of variation of its basic parameters. The essentials of the technique are provided in [14].

## 4. Application of HLS assimilation technique for assessment of the maximum wind speed from satellite and radar data

### 4.1 HLS assimilation approximation of spiral rainbands applied to satellite IR images

#### 4.1.1 Typhoon Phanfone (2002)

The first attempt to apply the HLS assimilation approximation to spiral rainbands on satellite IR images was undertaken by exploring data from the GMS-5 geostationary satellite during the monitoring of typhoon Phanfone existing in the Pacific Northwest in August 2002 [13]. The source of satellite data was the archive of IR images from the Naval Research Laboratory (NRL, USA; [http://www.nrlmry.navy.mil/sat\\_products.html](http://www.nrlmry.navy.mil/sat_products.html)). Meteorological data were taken from the Navy/Air Force Joint Typhoon Warning Center (JTWC-WP; Hawaii, USA) and Regional

Specialized Meteorological Center (RSMC-JMA; Tokyo, Japan). IR spiral rainband patterns pertain to the top of cyclone's cloud system (280–230 hPa, altitude 10–12 km). The rationale for comparison of the MWS resulted from the HLS processing with the best track data is the same as mentioned above.

Twenty-one images were processed which corresponded to the period from 21:31 UTC on August 14, 2002, till 12:31 UTC on August 18, 2002. Their results were subsequently united to six estimates. The length of the period covered by the analysis was 84 h. The estimates of the MWS are used to identify the stages of intensification and weakening of TC which are satisfactorily synchronized with the respective data of the Navy/Air Force Joint Typhoon Warning Center (JTWC). The correlation with data of the Regional Specialized Meteorological Center (RSMC-JMA) is observed only for the stage of intensification. Data of JTWC did not correlate either with RSMC data at the stage of TC weakening. In terms of the absolute value of the MWS, JTWC data exceed RSMC data for the moment of maximum TC intensification. It should be noted that data of the mentioned meteorological services differ from each other by 33% in terms of maximum TC intensity. The estimates of the MWS based on the HLS approximation occupy intermediate position between the above data. A detailed description of this study is given in [13].

#### 4.1.2 Hurricane Rita (2005)

In the current paper, an example of application of the HLS enhanced assimilation technique under processing IR images of a TC is provided exploring observation data of Hurricane Rita (AL182005) from geostationary satellite GOES-10 when the hurricane was in Gulf of Mexico. An image acquired at 6:30 UTC 23 September 2005 has been processed (**Figure 8**).

The image contains two spiral rainbands. They are the outer impressive band that starts from the northwest corner of the image and the inner one that starts from the north. Both bands reach the core of the cyclone close to its south sector. The radius of maximum wind has been assessed to be 70 km as a distance from the eye's

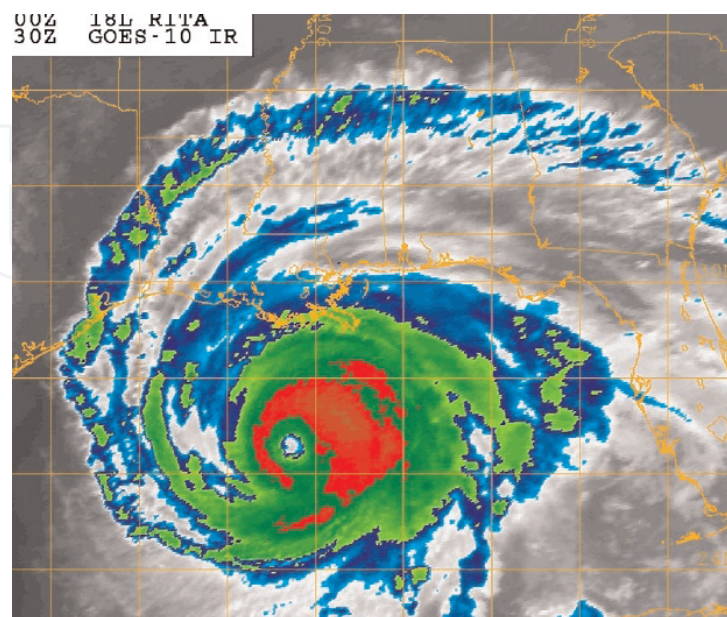


**Figure 8.**

IR image of Hurricane Rita 09/23/2005 at 06:30 UTC (eye center location: 26.58° N; 90.53° W) from GOES-10 geostationary satellite; source: Naval Research Laboratory (NRL, USA; [http://www.nrlmry.navy.mil/sat\\_products.html](http://www.nrlmry.navy.mil/sat_products.html)); file name, 20050923\_0630\_goes10\_x\_ir1km\_18LRITA\_120kts-924mb-265 N-907 W; original geographic grid is applied at intervals of two degrees; color temperature scale (roughly), blue is “–40° C,” green is “–60°C,” and red is “–70°C.”

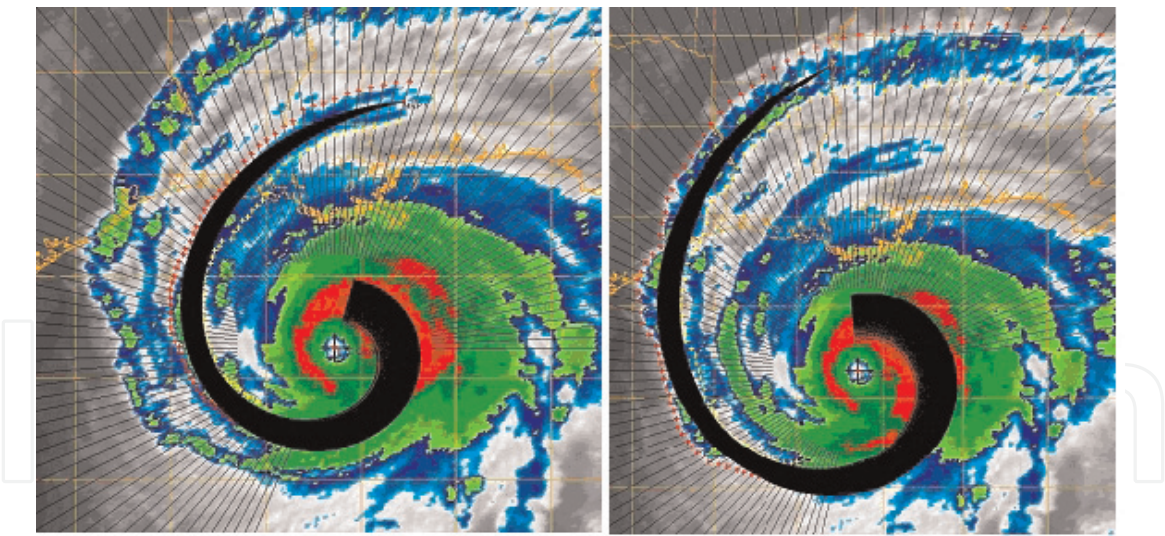


**Figure 9.** Illustration of HLS approximation (black spiral sector) of inner rainband (left picture) and the west sector of outer rainband (right picture) shown in **Figure 8**.

Rainband	Maximum wind speed, kts	
	Modal MWS derived from HLS approximation	Best track*
Inner band	117.7 ± 8.7	115
Western sector of outer band	114.1 ± 13.6	

\*Extrapolated from [25].

**Table 1.** Maximum wind speed derived from HLS approximation in comparison with the best track data of hurricane Rita.

center to the middle of a convective eyewall. Illustrations of the HLS approximation of both rainbands are provided in **Figure 9**. Resulted maximum wind speeds in comparison with the best track data [25] are presented in **Table 1**.

Following the HLS technique feature that presumes to use for approximation a signature closest to the TC core (where a streamline impact on cloud organization is most pronounced), the western sector of the outer rainband was approximated only. As follows from **Table 1**, the approximation of both rainbands results in the modal maximum wind speeds close to the best track speed with the acceptable accuracies (less than 12%). It should be noted that among other things, this illustrative example also shows the possibility of increasing the reliability of the HLS approximation by combining multiband estimates. In particular, the combined weighted estimate of MWS based on the data provided in **Table 1** is  $116.6 \pm 7.4$  kts.

**4.2 HLS assimilation approximation of spiral rainbands applied to airborne and coastal radar images**

**4.2.1 Comparison of operational and HLS estimates of the intensity of TC Irma (AL112017) based on the airborne and the best track data**

Maximum wind speeds in Hurricane Irma (AL112017) were estimated in [14] using its rainband radar signatures acquired by the NOAA Hurricane Research Division during routine aircraft missions into the hurricane. Most appropriate radar and other accompanied data were taken from the NOAA Hurricane Research Division (HRD) archive acquired for Hurricane Irma (AL112017) that existed in the

Atlantic basin from August 30 to September 12, 2017, and reached category 5 intensity. The radar data from airborne radars were taken from the HRD’s Atlantic Oceanographic and Meteorological Laboratory (AOML) website ([http://www.aoml.noaa.gov/hrd/data\\_sub/radar.html](http://www.aoml.noaa.gov/hrd/data_sub/radar.html)). The best track and aircraft data were taken from the National Hurricane Center’s Tropical Cyclone Report [26]. The data pertain to one of eight aircraft missions to the cyclone. This mission was conducted from morning to afternoon September 5, 2017. The numerical outcomes of the HLS approximation are listed in **Table 2**.

The data of the first two time points were acquired at altitude from 5 km to 6 km, the six others from 2 km to 3 km. At the higher altitude, the MWS was approximately from 80 kts to 100 kts; at the lower level, the mean modal wind speed was about  $161 \pm 5$  kts. This estimate is for a middle time point at approximately 10:45 UTC September 5 and manifests the maximum TC intensity that was estimated by the HLS approximation of all period of the HLS application from 21:16 UTC September 3 till 23:51 UTC September 8. As follows from [26], the wind speed of 164 kts measured directly by the aircraft at the flight level occurred approximately 10 h later. The best track MWS, which is for 10 m altitude, was about 150 kts. As per the best track data, the maximum intensity was 154 kts from noon September 5 to approximately 18:00 UTC September 6. The HLS estimates for this period are provided in [14] and amounted to 158–146 kts. These results indicate the satisfactory agreement of the HLS approach with in situ data (compare 161 kts and 164 kts). Lower speeds evaluated at high levels (two first time points in **Table 2**) follow the contemporary understanding of the vertical tangential wind profile in a TC (e.g., [24]) that presumes the decreasing of the wind speed up from the level of the maximum wind at altitude approximately 1–1.3 km (850–900 mb). The average error of the HLS approximation for the entire observation time ( $\sim 130$  h) of the comparative analysis with the best track data given in [14] was no more than 5%.

4.2.2 *The maximum wind speed in TC Irma (2017) by the HLS approximation of the rainband signatures from the coastal San Juan radar in comparison with best track data*

During the passage of the TC Irma near the island of Puerto Rico, the cyclone was in the survey zone of the weather radar WSR-88D installed in the city of San Juan. The base for processing was the reflectivity image at 21:15 UTC 6 September

Time point no.	Altitude, m	UTC	Observation time, hours	V <sub>m,mdl</sub>		Error V <sub>m,mdl</sub>		R <sub>m</sub> , km
				m s <sup>-1</sup>	kts	m s <sup>-1</sup>	kts	
22	6089	8:41:44	56.68	53	103.0	2.0	3.9	30
23	5244	8:47:58	56.78	40	77.8	3.0	5.8	26
24	2999	9:27:39	57.45	75.5	146.8	2.5	4.9	34
25a	2999	9:43:20	57.72	76	147.7	4	7.8	33
25b	3000	9:48:04	57.80	89	173.0	1	1.9	30
26	2510	10:31:26	58.52	79	153.6	3	5.8	34
27	2369	11:01:38	59.02	89	173.0	7	13.6	30
28	2531	12:01:32	60.02	88	171.4	4	7.8	31

**Table 2.**  
*Results of the HLS approximation of radar spiral signatures of TC Irma acquired during airborne sounding on September 5, 2017 (collection index 20170905H1).*

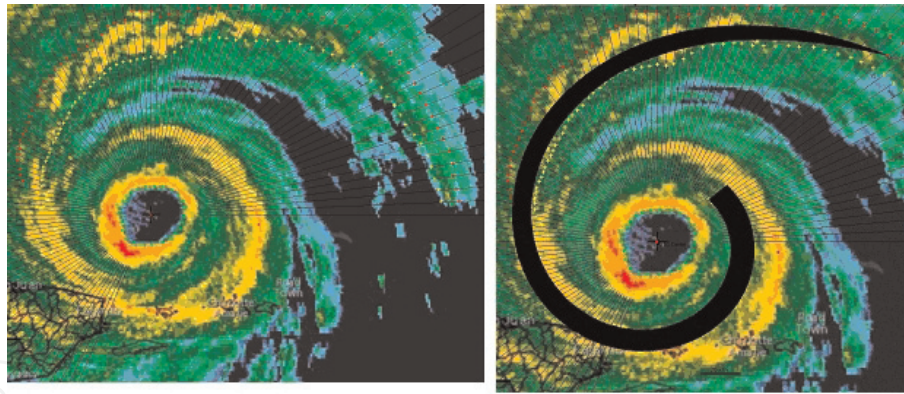


**Figure 10.**

*Left image—reflectivity image of TC Irma from San Juan WSR-88D (2115 UTC September 6, 2017 [26]); right image—illustration of HLS approximation of the NW rainband.*

2017 that is shown in **Figure 10** (left image) when the TC center was located at  $18.9^{\circ}$  N/ $65.4^{\circ}$  W [25]. The image refers to the beginning of the cyclone weakening stage and has the double eyewall structure that indicates a double wind maximum. Under the HLS approximation, the RMW was selected within the outer eyewall, as follows from findings in [27, 28], and estimated to be about 62 km.

The modal and mean maximum wind speeds estimated from the HLS approximation of the northwest rainband (**Figure 10**, right image) were  $74 \text{ m s}^{-1}$  (143.9 kts) and  $75.4 \text{ m s}^{-1}$  (146.6 kts), respectively. Accordingly, these speeds are approximately by 6 kts and 3 kts lower than the best track speed 150 kts at this time.

## 5. Summary

A new approach to use the characteristics of spiral cloud-rain bands of a tropical cyclone, observed by ground-based and aircraft radars, as well as satellites in visible and infrared wavelengths, is considered. The physical substantiation of the proposed approach is (1) the assumption about the orientation of the SCRBs mainly along the streamlines and (2) the analytically derived streamline equation in the form of the hyperbolic-logarithmic spiral. It is shown that the logarithmic spiral usually used to describe the configuration of SCRB is only a special case of the HLS. Unlike the empirically applying logarithmic spiral, the HLS coefficients depend on the MWS and the friction factor. The analysis of changes in the configuration of the HLS depending on the intensity of a TC is conducted. An explanation for experimentally observed phenomenon of the “rounding” of the SCRB (i.e., a decrease in the crossing angle) with increasing intensity of the TC as a whole, as well as with approaching to the radius of maximum wind, is proposed. The similarity of the SCRB configuration to the logarithmic spiral in some cases is interpreted also. The technique for approximation of a SCRB in the form of the HLS based on the least squares method and on the assimilation procedure was developed for obtaining MWS estimates at the height of the SCRB location. Testing of the proposed approach was performed based on literature data from ground-based coastal and aircraft radars, data of regular aircraft reconnaissance missions in the TC, and satellite data available via the Internet. A certain disadvantage of the method is its applicability, as a rule, for mature tropical cyclones, where its cloudy field manifests well-defined SCRBs and a clearly defined circulation center (eye center). On the other hand, the physically based configuration of a SCRB as the hyperbolic-logarithmic spiral allows one to develop the method for estimating the position of the circulation center with the eye covered with clouds, examples of which are

given in [11, 13]. The results obtained suggest that the development and improvement of the proposed approach will make it possible to use the radar and satellite information more fully to assess the physical characteristics of a TC. The HLS approach to retrieve the TC's intensity is particularly benefited for ground-based coastal radar probing of a TC before its landfall and the absence of aircraft reconnaissance missions.

IntechOpen


IntechOpen

### **Author details**

Boris Yurchak  
Environmental Protection Agency, Washington D.C., USA

\*Address all correspondence to: [yurchak.boris@epa.gov](mailto:yurchak.boris@epa.gov)

### **IntechOpen**

© 2019 The Author(s). Licensee IntechOpen. This chapter is distributed under the terms of the Creative Commons Attribution License (<http://creativecommons.org/licenses/by/3.0>), which permits unrestricted use, distribution, and reproduction in any medium, provided the original work is properly cited. 

## References

- [1] Dvorak VF. Tropical cyclone intensity analysis and forecasting from satellite imagery. *Monthly Weather Review*. 1975;**103**:420-430
- [2] Olander TL, Velden CS. The advanced Dvorak technique: Continued development of objective scheme to estimate tropical cyclone intensity using geostationary infrared satellite imagery. *Weather and Forecasting*. 2007;**22**: 287-298
- [3] Wexler H. Structure of hurricanes as determined by radar. *Annals of the New York Academy of Sciences*. 1947;**48**: 821-844
- [4] Senn HV, Hiser HW, Bourret RC. Studies of Hurricane Spiral Bands as Observed on Radar. National Hurricane Research Project. U.S. Department of Commerce. Report No. 12; 1957. 13 p
- [5] Fung IY. The organization of spiral rain bands in a hurricane. Doctoral dissertation thesis. Massachusetts: Massachusetts Institute of Technology; 1977. 140 p
- [6] Fernandez W. Organization and motion of the spiral rainbands in hurricanes: A review. *Ciencia y Tecnología*. 1982;**6**(1-2):49-98
- [7] Houze RA Jr. Clouds in tropical cyclones. *Review. Monthly Weather Review*. 2010;**138**:293-344
- [8] Wang Y. Recent research progress on tropical cyclone structure and intensity. *Tropical Cyclone Research and Review*. 2012;**1**(2):254-275
- [9] Lahiri A. A study of cloud spirals of tropical cyclones. *Mausam*. 1981;**32**(2): 155-158
- [10] Burton A, Velden C. Curved band patterns. In: *Proceedings of the International Workshop on Satellite Analysis of Tropical Cyclones*. Report Number TCP-52. Honolulu, Hawaii, USA: World Meteorological Organization; 2011, 2011. pp. 65-67
- [11] Yurchak BS. Description of cloud-rain bands in a tropical cyclone by a hyperbolic-logarithmic spiral. *Russian Meteorology and Hydrology*. 2007; **32**(1):8-18
- [12] Yurchak BS. Formula for spiral cloud-rain bands of a tropical cyclone. In: *Proceedings of the 28th Conference on Hurricanes and Tropical Meteorology*. Orlando, FL; 2008, 2008. 5 p. Available online: [http://ams.confex.com/ams/28Hurricanes/techprogram/programexpanded\\_471.htm](http://ams.confex.com/ams/28Hurricanes/techprogram/programexpanded_471.htm)
- [13] Yurchak BS. Estimation of tropical cyclone intensity from the satellite infrared images of its spiral cloud bands. *Russian Meteorology and Hydrology*. 2018;**43**(9):581-590
- [14] Yurchak BS. An estimate of the hurricane's intensity from radar data using hyperbolic-logarithmic approximation. *International Journal of Remote Sensing*. 2019. DOI: 10.1080/01431161.2019.1635288
- [15] Willoughby HE, Marks FD, Feinberg RJ. Stationary and moving convective bands in hurricanes. *Journal of the Atmospheric Sciences*. 1984; **41**(22):3189-3211
- [16] Willoughby HE. The dynamics of the tropical cyclone core. *Australian Meteorological Magazine*. 1988;**36**:183-191
- [17] Batchelor GK. *An Introduction to Fluid Dynamics*. Cambridge: Cambridge University Press; 1967. 634 p
- [18] Guralnik II, Dubinskii GP, Mamikonova SV. *The Meteorology. Handbook for Colleges*.

Gidrometeoizdat, Leningrad, 1972. 416 p.[in Russian]

[19] Wendell HE. Meteorology-Theoretical and Applied. Kennelly Press. (Copyright, 1944 by Hewson EW and Longley RW); 2007. 468 p

[20] Anthes RA. Tropical cyclones. Their evolution, structure and effects. AMS, Meteorological Monographs. 1982; **19**(41):210

[21] Powell MD, Vickery PJ, Reinhold TA. Reduced drag coefficient for high wind speeds in tropical cyclones. *Nature*. 2003;**422**:279-283

[22] Frank WM. The structure and energetics of the tropical cyclone I. storm structure. *Monthly Weather Review*. 1977;**105**:1119-1135

[23] Franklin JL, Lord SJ, Feuer SE, Marks FD Jr. The kinematic structure of hurricane gloria (1985) determined from nested analysis of dropwindsonde and doppler radar data. *Monthly Weather Review*. 1993;**121**:2433-2450

[24] Franklin JL, Black ML, Valde K. GPS dropwindsonde wind profiles in hurricanes and their operational implications. *Weather and Forecasting*. 2003;**18**:32-44

[25] Knabb KD, Brown DP, Rhome JR. Tropical Cyclone Report Hurricane Rita, 18–26 September 2005. National Hurricane Center; 2006. 36 p. Available online: [https://www.nhc.noaa.gov/data/tcr/AL182005\\_Rita.pdf](https://www.nhc.noaa.gov/data/tcr/AL182005_Rita.pdf)

[26] Cangialosi JP, Latta AS, Berg R. National Hurricane Center Tropical Cyclone Report. Hurricane Irma (AL112017). 30 August-12 September 2017; 2018. 111 p. [http://www.aoml.noaa.gov/hrd/Storm\\_pages/irma2017/index.html](http://www.aoml.noaa.gov/hrd/Storm_pages/irma2017/index.html)

[27] Willoughby HE, Clos JA, Shoreibah MG. Concentric eye walls,

secondary wind maxima, and the evolution of the hurricane vortex. *Journal of the Atmospheric Sciences*. 1982;**39**(2):395-411

[28] Samsury CE, Zipser EJ. Secondary wind maxima in hurricanes: Airflow and relationship to rainbands. *Monthly Weather Review*. 1995;**123**:3502-3517